Supplementary Materials

Evaluation of Techniques used for Visualisation of Hydrogel Morphology and Determination of Pore Size Distributions

Imanda Jayawardena[1], Petri Turunen[2,3], Bruna Cambraia Garms[1], Alan Rowan[3], Simon Corrie[4], Lisbeth Grøndahl[1,3] *

1. School of Chemistry and Molecular Biosciences, University of Queensland, Brisbane, QLD 4072, Australia.

2. Microscopy Core Facility, Institute of Molecular Biology, Mainz, Germany

3. Australian Institute for Bioengineering and Nanotechnology, University of Queensland, Brisbane, QLD 4072, Australia

4. Department of Chemical Engineering, ARC Centre of Excellence in Convergent Bio-Nano Science and Technology, Monash University, Clayton, VIC 3800, Australia.

Example of raw and deconvolved CLSM and STED images:

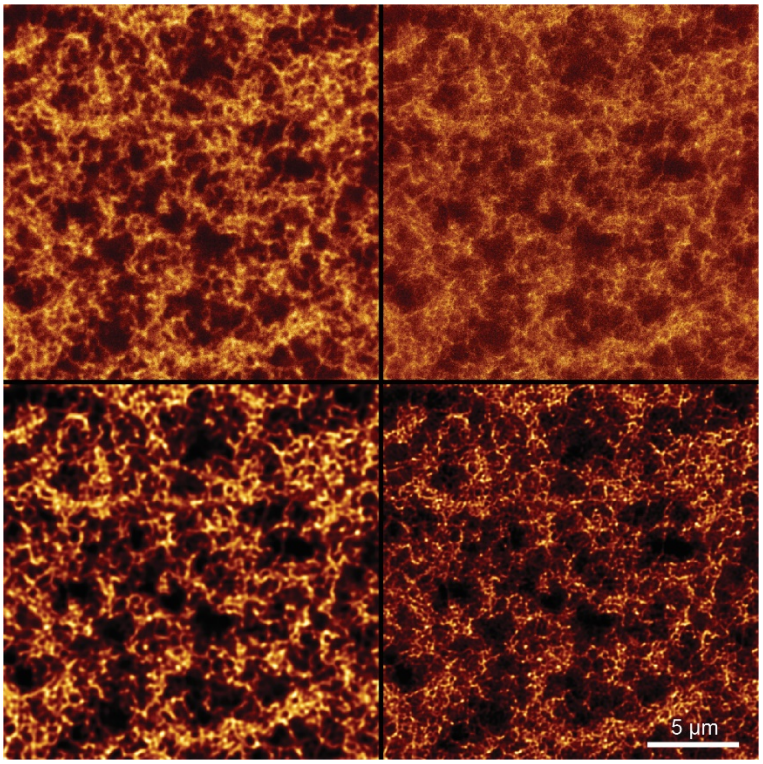

Figure S1. Comparison of raw and deconvolved images of CLSM and STED microscopy of 0.38% agarose gel. (Top Left) CLSM raw. (Bottom Left) CLSM deconvolved (Top Right) STED raw, (Bottom Right) STED deconvolved (scale bar: 5 µm).

Examples of structures that can be visualised by Cryo-SEM or SEM after erroneous treatments:

Methods

Freeze drying Two 1.5% gel samples prepared using agarose A (gelling temperature; 34 – 38 °C) in PBS were freeze dried for 24 hours (Thermo Savant Micro Modulyo230 freeze drier, Pfeiffer ONF-16 vacuum pump) after which they were fractured to expose the interior surfaces of the gel. More than four regions of each sample were imaged with a JEOL JSM-7100F Field Emission Scanning Electron Microscope, at a low accelerating voltage (e.g. 2 kV) and a spot size of 3. These samples were not subjected to pore size determination.

Critical point drying (CPD) Samples of 1.5% agarose gel for SEM were subjected to critical point drying in a Tousimis AUTOSAMADRI-815 critical point dryer using a modified version of the manufacturer's Stasis Mode technique (Tousimis AUTOSAMADRI-815 - Processing Thick Samples using Stasis Mode). Prior to critical point drying, agarose gels were cut into approximately 1 mm x 1 mm x 1 mm sections. Dehydration was carried out in a series of graded ethanol/water solutions (30 wt% to 90 wt% in 10% stepwise increments), where the sample was held for an hour in each solution, and twice in 100% ethanol where the sample was held overnight in-solution. After the final dehydration step, samples were placed in porous specimen pots (KCPD800A Proscitech) while in 100% ethanol and loaded into the CPD process chamber. The chamber was flooded with liquid CO_2 and the samples were left in Stasis mode for 3 hours at room temperature prior to heating the process chamber. CPD dried samples were sputter coated twice with Pt for 120 s at 10 mA (circa 10 to 20 nm coating thickness) and then imaged using a JEOL JSM-7100F Field Emission Scanning Electron Microscope at 2 to 5 kV and probe current 3 to 5 equipped with a JEOL secondary electron detector (LED).

Liquid Ethane Freezing 1.5% agarose gels prepared with agarose A (gelling temperature; 34 – 38 °C) in PBS, were cut out to reach a sample thickness of approximately 5 mm – 1 cm, in order to obtain a freezing depth of 30 µm offered by the liquid ethane freezer (according to manufacturer's details). The samples were frozen by rapidly plunging them into liquid ethane. Images were obtained using a JEOL JSM-7100F Field Emission Scanning Electron Microscope, at 2 to 5 kV, and probe current 3 to 5 equipped with a JEOL secondary electron detector (LED).

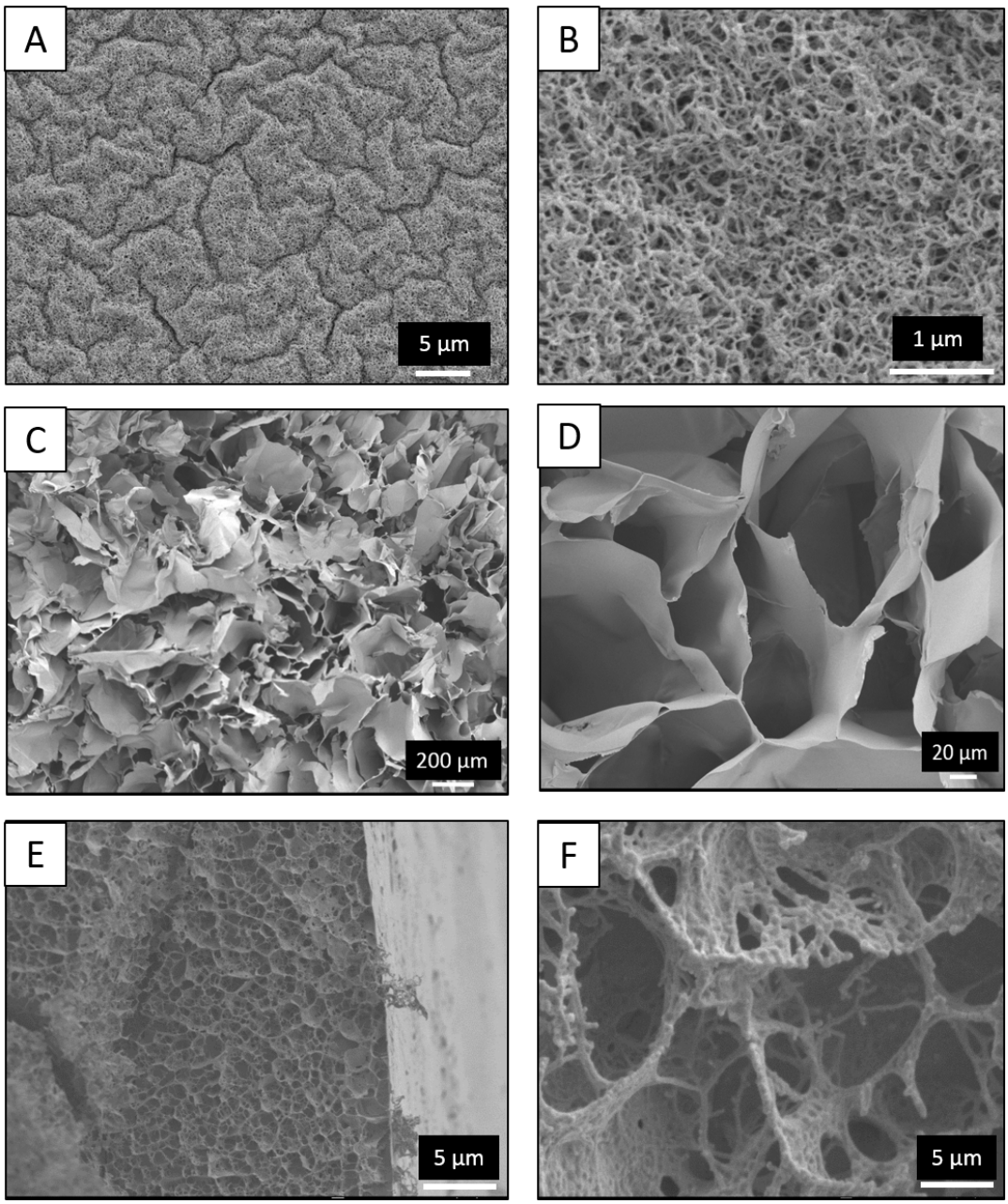

Figure S2. SEM images of 1.5% agarose gels prepared using agarose A in PBS prepared using CPD at (A) 3,000x and (B) 30,000x magnifications, freeze drying at (C) 50x (D) 400x and LE freezing at (E) 3,000x and (F) 30,000x magnifications depicting the distortion of the native hydrogel structure

Results

Figure S2 give examples of images of agarose hydrogels displaying artefacts. Figure S2A and B display the irregular contraction caused by CPD at two magnifications where the higher magnification is that used in the main document. This contraction cause channel-like structures to appear and these are not present when using HPF (see main manuscript). In Figures S2C and

D, a sheet like morphology is seen and the apparent pores of > 20 µm are caused by freezing artefacts introduced by freeze-drying. In Figures S2E and F, a distorted hydrogel morphology is observed with micron-sized pores due to the relatively slow freezing at ambient pressure when using liquid ethane. None of these methods are recommended for the preparation of hydrogels where the native hydrated structure is to be visualised. Please see the main manuscript for details of correct gel preparation.

Pore size determination using the manual approach:

A circle drawn using the ImageJ software was placed within the walls of the pore in a manner to achieve the largest circle possible and its area was determined to obtain the pore diameter. The scale bar of each SEM/AFM/STED image was used as the calibration reference, and the area of this circle was calculated through the software, which led to the calculation of the pore diameter. An example is shown in Figure S3.

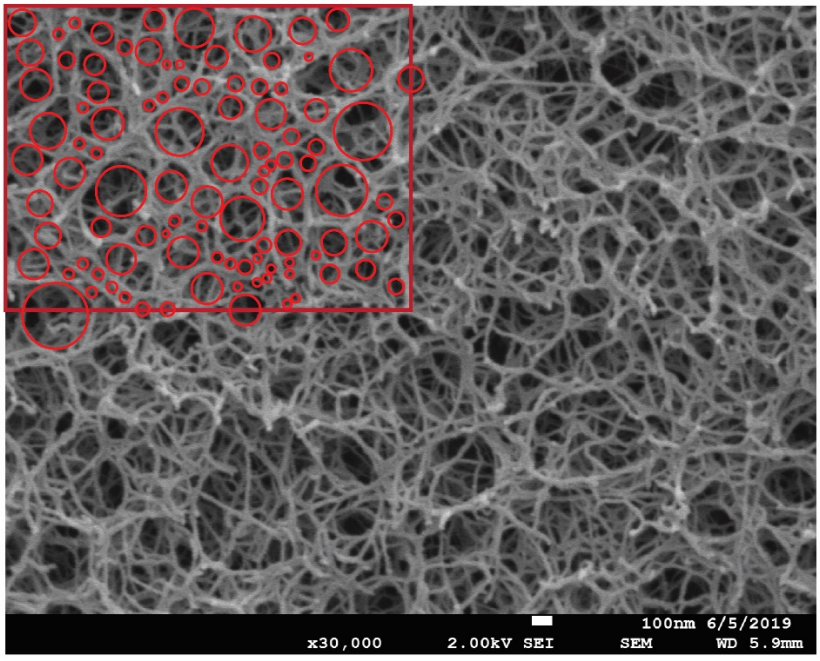

Figure S3. SEM image of a 0.38% agarose gel prepared in water. Pores used to find the pore size distribution is highlighted in one quadrant as an example.

Pore size determination using intensity plots:

Intensity plots were extracted from data generated by AFM. A horizontal line was drawn through the centre of a chosen pore (Figure S4A), then an intensity plot of the line was generated (Figure S4B). Pores were identified from the line plot, as the troughs in the plot that corresponded to the coordinates on the AFM image. This process is generally not automated and as such, bias may be introduced. A threshold that defines where the pore wall ends and the pore void starts was chosen as described in the main manuscript. We interpret the yellow to orange regions in the AFM image (Figure S4A) as the pore walls and regions appearing black or dark purple (z-dimensions of -60 to -30 nm) as the pores. When importing the images into ImageJ/FiJi these z-dimensions are converted into grey values ranging from 0 to 255 which are unitless measures of pixel brightness. This scale is in turn a representative of the z-dimensions ranging from -60 to 60 nm in the AFM images. The effect of choosing two different thresholds was evaluated for one set of AFM data as illustrated in Figure S4B.

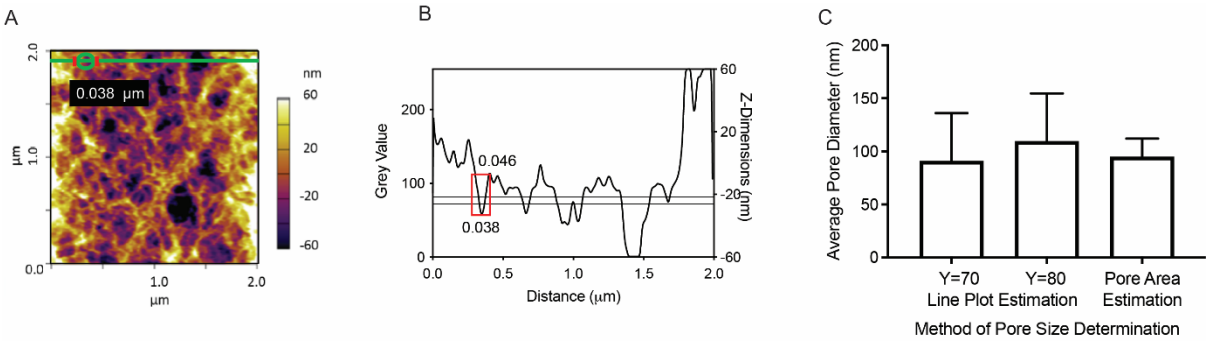

Figure S4. (A) An AFM image of a 1.5% gel prepared in PBS, including a schematic representation of the identified pore circled (green). The demarcations on either side of the pore indicate the manual pore size estimation method, while the horizontal line drawn across the centre of the pore indicates the line plot estimation method. (B) An example of a height intensity plot generated for the selected pore, indicating the two thresholds from the left y-axis corresponding to grey values used for pore size comparison. The pore sizes are 38.0 nm (0.038 µm) at Y=70 and 46.0 nm (0.046 µm) at Y=80. (C) Graph indicating the average pore size and standard deviation from pore size data obtained from the two thresholds indicated in (B) as well as using the manual pore size estimation method. Mann-Whitney tests indicated no significant difference between the PSD data from the two thresholds ($p = 0.32$, $n = 10$). Mann-Whitney tests indicated no significant difference between the PSD data from the two methods ($p = 0.8386$, $n = 10$); pore size data obtained from the intensity line plot and the method of placing a circle onto pores of the image.

These threshold values were chosen such that every pore was captured with both thresholds. The pore size values are shown in Figure S4C indicating no statistical difference between the two. This highlights that although a bias is associated with arbitrarily deciding upon a threshold, the error introduced is acceptable. Intensity plots for each analysed pore are included in the Supplementary file as Figure S7.

For images obtained by AFM, pore depth measurement is an inherent part of the resultant image, thus, in this case, pores were defined based on a depth threshold. For the determination of the pore size based on AFM data, the two approaches, intensity plot and manual approach were compared for the 1.5% agarose gel (Figure S4C). Using the same threshold for both approaches, it was found that there was no statistical difference and as such either approach is equally valid.

Binarisation of deconvoluted STED images:

The deconvoluted microscopy image was subjected to binarisation, by manually selecting a threshold using the Fiji software[1]. The choosing of an appropriate threshold is difficult as recognised previously.[2] One issue with choosing a single (global) threshold is that it is only suitable for images which have a homogenous background. However, for the hydrogel images captured by STED, there is a very low background in the large pore areas, but in more dense areas there is a higher background as a result of a denser network. Similar to the approach used by Vandaele et al.[2], we assessed by visual inspection the quality of different thresholds.

We have found that the 60% binarisation threshold (Figure S5 right) was most visually optimal for the manual approach (as indicated by the square) due to its close resemblance to the deconvoluted STED image (Figure S5 left). The video shows the series of thresholds applied to identify the optimal threshold.

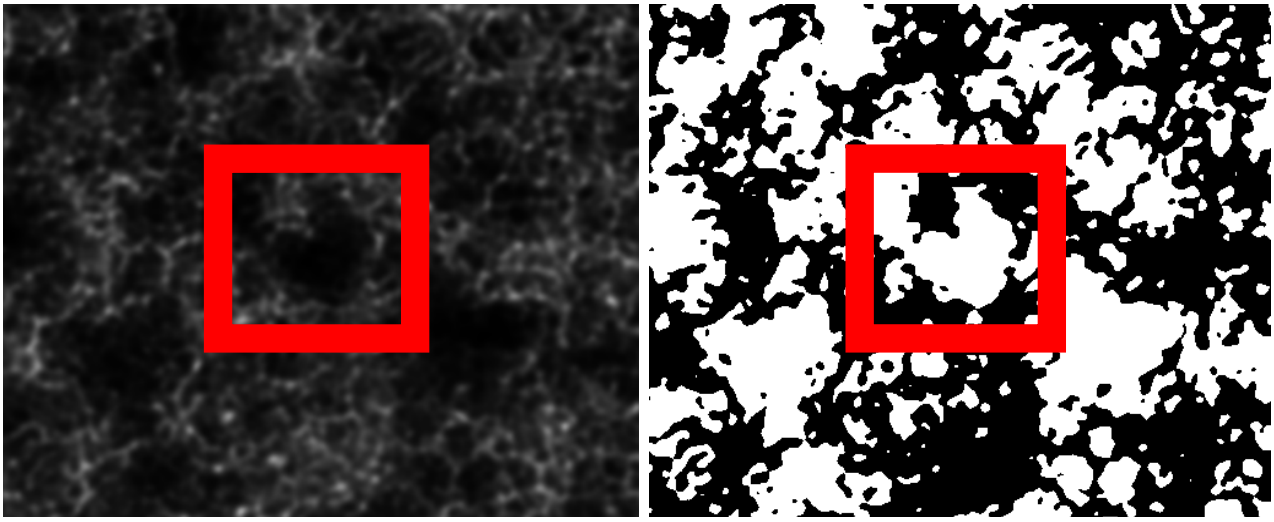

Video illustrating applying different thresholds to the image in left panel has been provided with this submission.

Figure S5. STED microscopy image of a 0.38 % agarose hydrogel. Left: Deconvoluted image, Right: binarized image using the 60% threshold. The square highlights an area with an identified pore.

Determination of PLGA particle size in composite hydrogel:

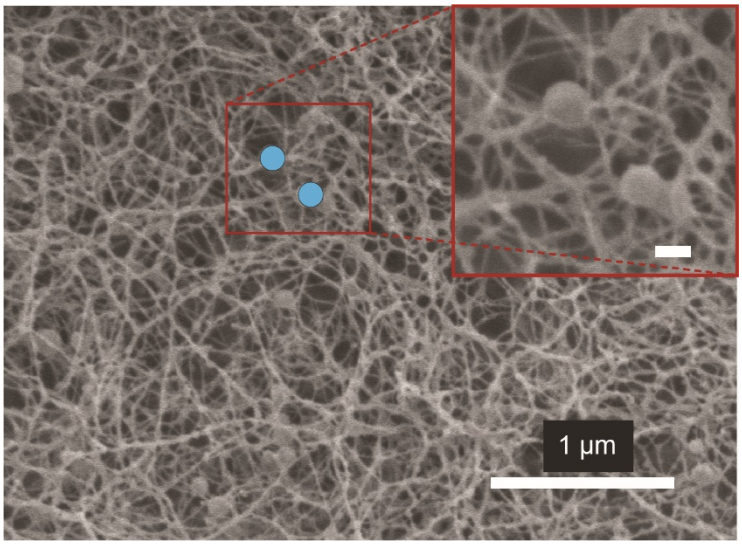

Figure S6. Cryo-SEM of 0.38% agarose hydrogel with PLGA nanoparticles at 30,000× (main figure), and 60,000× magnification (inset) of selected region. The closed circle drawn in blue illustrates how the size of the nanoparticle is defined using the manual approach. Scale bar: 1 µm and 100 nm for the main image and inset, respectively. A description of the approach used is included in the main document.

Intensity plots from AFM images:

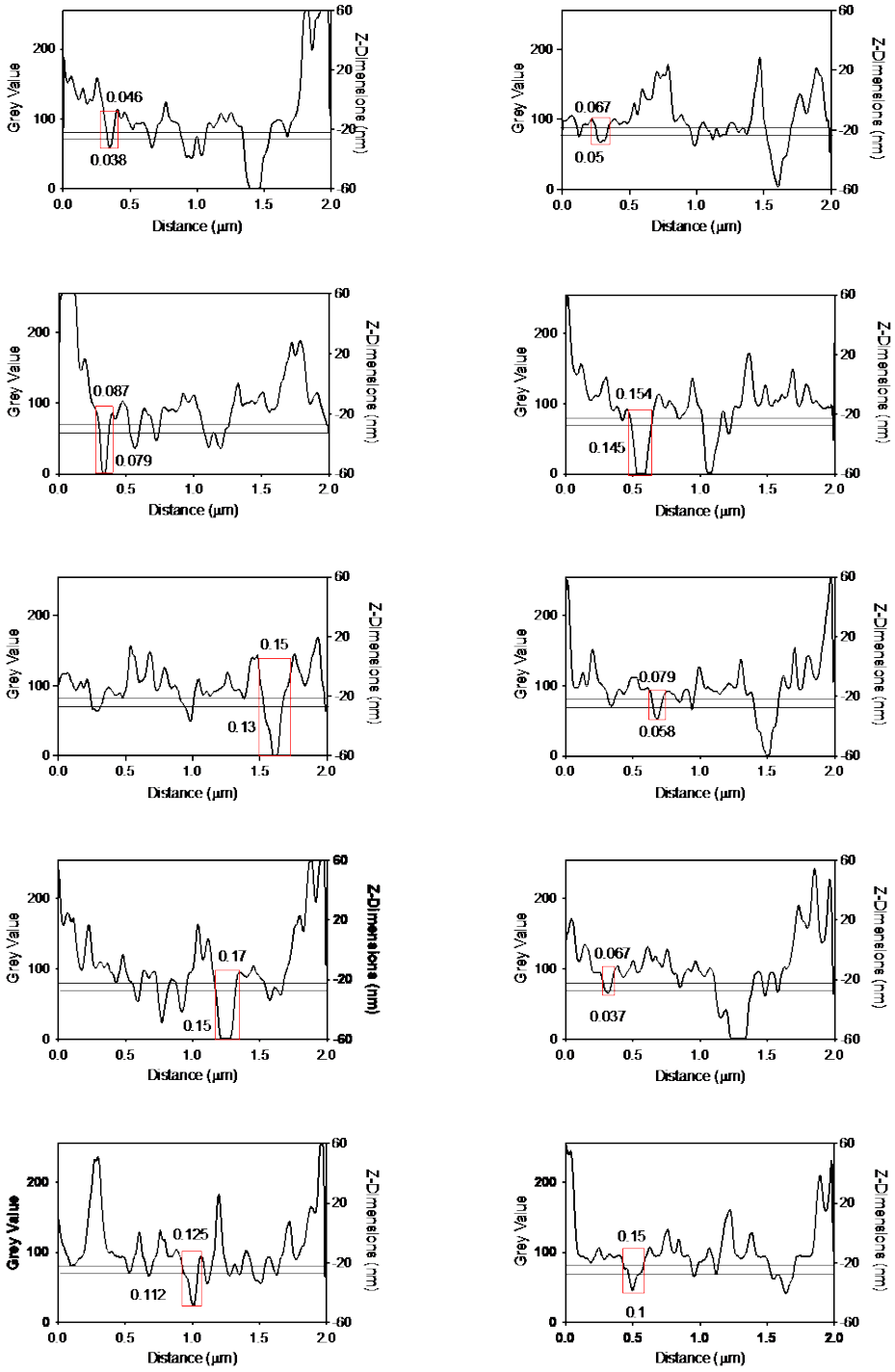

Figure S7. Intensity plots, acquired via the ImageJ software, of a 1% agarose hydrogel network captured via AFM imaging. The sections outlined in red indicate the pore under consideration for the given line plot.

Evaluation of bundle thickness:

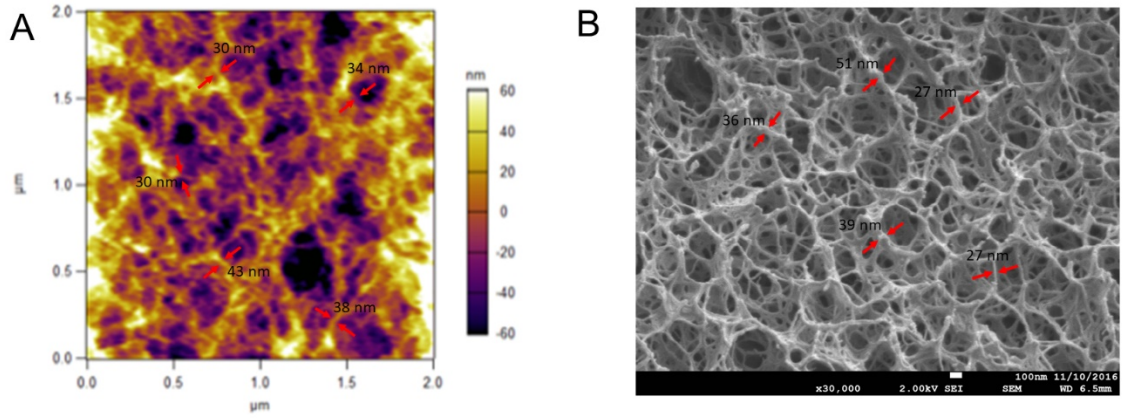

Figure S8. Estimation of bundle thickness for (A) 1.5% gel imaged via AFM, (B) 1.0% gel imaged via Cryo-SEM. Each pair of red arrowheads indicate the bundle whose thickness was measured.

Cryo-SEM data for additional gel samples (1.5% replicate):

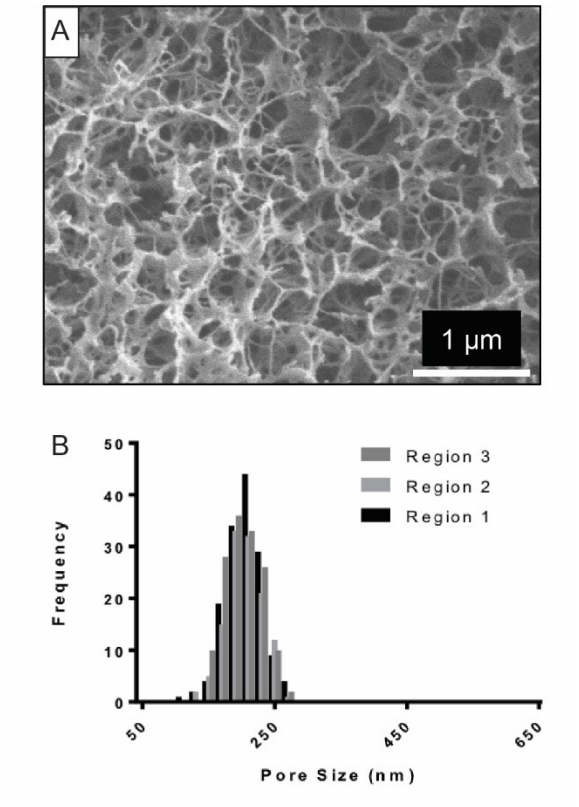

Figure S9. Cryo-SEM images of agarose gel sample prepared as described in main document at 30,000× magnification (scale bar: 1 µm). (A) 1.5% true replicate. Respective combined pore size distribution obtained from four regions of the sample (B).

Cryo-SEM data for additional gel samples (1.0% different agarose type; water vs PBS):

Materials: Agarose for immune-electrophoresis, low EEO: Agarose A (gelling temperature 34-38°C, Product Number: A4679, Catalogue Number: US024566, Sigma-Aldrich), high gelling temperature agarose: Agarose B (type VI-A, gelling temperature 39.5°C-42.5°C, Product Number: A7174, Catalogue Number: US025022 Sigma- Aldrich) and low gelling temperature agarose: Agarose C (type VII-A, gelling temperature 24°C-28°C, Product Number: A0701, Catalogue Number: US021454 Sigma- Aldrich), 1 × Phosphate Buffered Saline (PBS) diluted from 10 × PBS (Bio-Whittaker), hexadecane (Merck) and deionized (DI) water were employed.

Results: The type of agarose (with different reported gelling temperatures) used for preparation of the gel was evaluated. Figure S10A-C display the Cryo-SEM images of agarose A, B and C; three types of agaroses with different gelling temperatures of 34°C – 38°C, 39.5°C – 42.5°C and 24°C– 28°C, respectively. The variation of the pore sizes in relation to the gelling temperature is plotted in the adjoining graph in Figure S10D. Kruskal-Wallis tests indicated significant differences among the mean pore diameters of the three different types of agarose gels (p-value < 0.0001). The smallest pore size range was observed for agarose A; at 225 ± 20 nm, followed by agarose B with a pore size range of 240 ± 20 nm. The largest pore sizes were exhibited by agarose C at 335 ± 20 nm. It can thus be concluded that relatively small pore sizes are observed for gels prepared using agarose of high gelling temperature (> 34 °C, agarose A and B) while a relatively large pore size is observed for gels made from agarose with low gelling temperature (< 30 °C, agarose C).

The solution composition that was used to prepare the agarose gel was evaluated. 1.0% agarose gels were prepared using either DI water or PBS buffer, and the pore size distributions of these gels were determined (Figure S10E and F). The pore size distribution for the gel prepared in DI water when subjected to Kruskal-Wallis tests indicated a significant difference (p-value < 0.0001) compared to the gel prepared in PBS, with the average values obtained for 1.0% agarose gels prepared in DI water gel at 140 ± 35 nm and for 1.0% agarose gels prepared in PBS at 230 ± 30 nm. This difference can be attributed to the differences in the ionic strengths of PBS (0.14 mol L^{-1}) and DI water (approximately 0 mol L^{-1}).

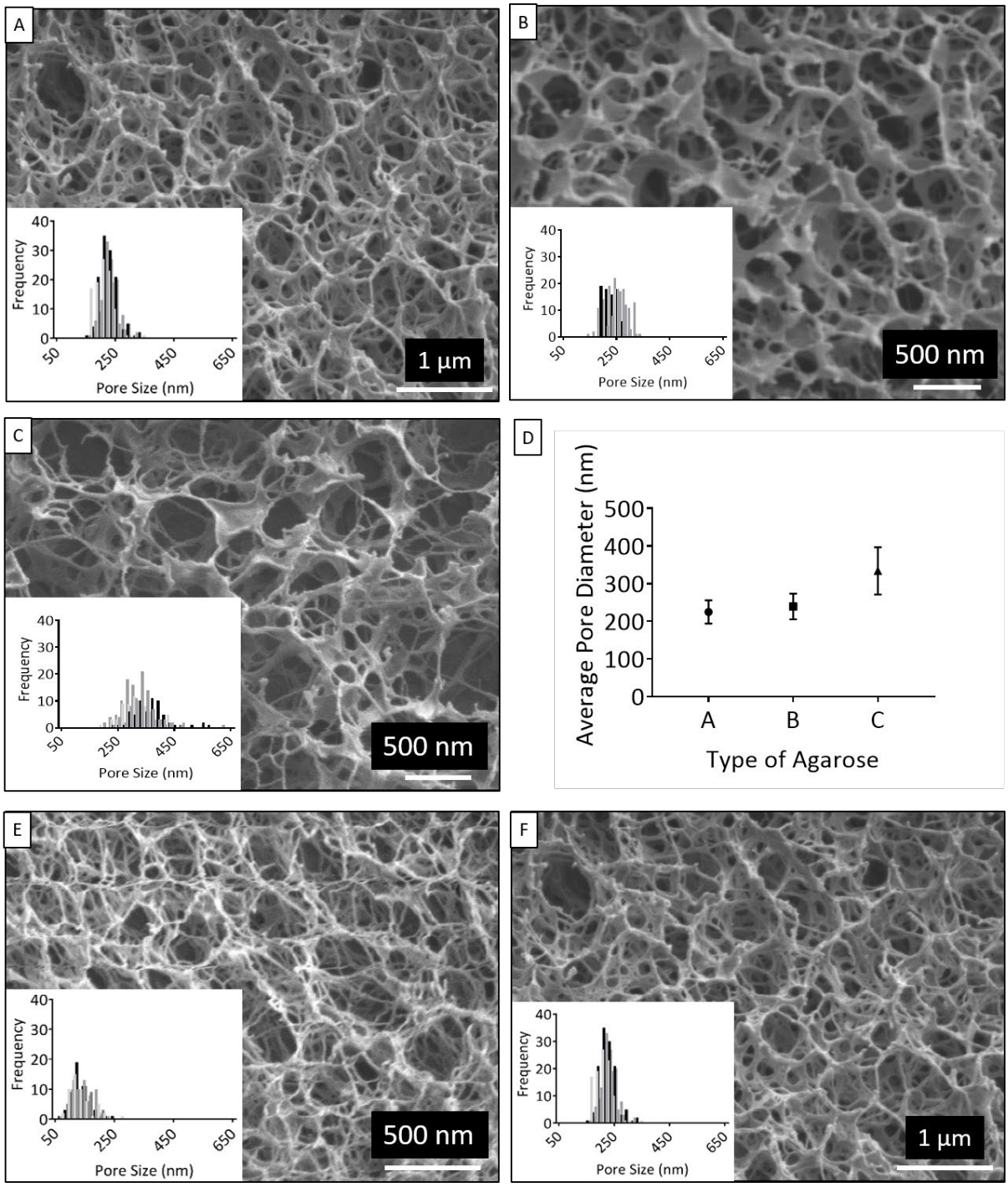

Figure S10. Effect of gel preparation conditions on agarose gel pore sizes. (A-D) Cryo-SEM images of 1% agarose gels with different gelling temperatures prepared in PBS. (A) Agarose A (gelling temperature; 34°C – 38°C) (B) Agarose B (gelling temperature; 39.5°C – 42.5°C) (C) Agarose C (gelling temperature; 24°C– 28°C) (D) Graph indicating the variation of pore size with agarose type (y-axis error bars correspond to standard deviations) (E-F) Cryo-SEM images and pore size distributions of 1% gels prepared using agarose A (gelling temperature; 34°C – 38°C) with different solution compositions; (E) MiliQ water (F) PBS.

Table S1. Examples of agarose pore size data of studies reported in the literature containing adequate gel preparation information.

Technique	Gelling temperature of agarose (ºC)	Solution	Agarose Conc. (%)	Pore Diameter (nm)
Direct Techniques				
AFM[3*]	17 [a]	PBS	0.75	935
			1	690
			1.5	480
			1.75	280
CLSM[4]	34 - 45 [b]	Distilled water	0.25	1550 ± 360
			0.5	990 ± 210
			0.75	730 ± 180
			1	560 ± 130
Indirect Techniques				
Absorbance[5*]	34.5-37.5 [c]	DI water	1	250
			1.5	150
			2	100
Turbidity[6]	34.5 - 37.5 [d]	Distilled water	2	100 ± 1
NMR[7]	26 - 30 [e]	DI water	0.08	240.0
			1.63	120.0
			2.25	86.9
			2.89	67.2
			3.68	52.3
			4.54	42.1
			4.59	41.6

Technique	Gelling temperature of agarose (ºC)	Solution	Agarose Conc. (%)	Pore Diameter (nm)
Particle tracking method[8*]	34.5−37.5 [f]	DI water	0.25	750
			0.5	500
			0.75	250
SPT analysis[9]	36ºC [g]	DI water	1	150 ± 130
			2	60 ± 120
fcsSOFI[9]	36ºC [g]	DI water	1	240 ± 90 1000 ± 500
			2	300 ± 100

[*] The individual data points were not provided. Tabulated values are approximate values inferred from the graphs provided.
a-g: Details of the agarose type/s used exactly as specified in the respective publication.
[a] SeaPrep Agarose (FMC, Rockland, ME), 60ºC melting temperature
[b] Agarose (CAS No. 9012−36−6) was purchased as fine white powder from Fisher Scientific GmbH with a specified gelling temperature
[c] SeaKem LE Agarose (high-melt, gelling temperature for 1.5%: 34.5-37.5 ºC) and Bio-Rad Certified low-melt agarose
[d] Purified Sigma sample (type I-A, low EEO, A-0169, lots 16H0343 and 56H1046), with a low ash (,0.5%) and sulfate contents (0.06%)
[e] Agarose (A-4018 type VII low temperature gelling) Sigma Chemicals St. Louis, MO
[f] Agarose was purchased from Fisher (Pittsburgh, PA) (molecular biology grade, low electroendosmosis, gelation temperature
[g] Agarose type I low EEO, Sigma-Aldrich

References

1. Schindelin, J.; Arganda-Carreras, I.; Frise, E.; Kaynig, V.; Longair, M.; Pietzsch, T.; Preibisch, S.; Rueden, C.; Saalfeld, S.; Schmid, B.; Tinevez, J.-Y.; White, D. J.; Hartenstein, V.; Eliceiri, K.; Tomancak, P.; Cardona, A., Fiji: an open-source platform for biological-image analysis. *Nature Methods* **2012,** *9* (7), 676-682.
2. Vandaele, J.; Louis, B.; Liu, K.; Camacho, R.; Kouwer, P. H.; Rocha, S., Structural characterization of fibrous synthetic hydrogels using fluorescence microscopy. *Soft Matter* **2020,** *16* (17), 4210-4219.
3. Peng, J.; Pan, Q.; Zhang, W.; Yang, H.; Zhou, X.; Jiang, H., Effects of DS-modified agarose gels on neurite extension in 3D scaffold through mechanisms other than changing the pore radius of the gels. *Journal of Biomedical Materials Research Part A* **2014,** *102* (7), 2157-2162.
4. Russ, N.; Zielbauer, B. I.; Koynov, K.; Vilgis, T. A., Influence of nongelling hydrocolloids on the gelation of agarose. *Biomacromolecules* **2013,** *14* (11), 4116-4124.

5. Narayanan, J.; Xiong, J. Y.; Liu, X. Y., Determination of agarose gel pore size: Absorbance measurements vis a vis other techniques. *J. Phys. Conf. Ser.* **2006,** *28* (1), 83-86.
6. Aymard, P.; Martin, D. R.; Plucknett, K.; Foster, T. J.; Clark, A. H.; Norton, I. T., Influence of thermal history on the structural and mechanical properties of agarose gels. *Biopolymers* **2001,** *59* (3), 131-144.
7. Chui, M. M.; Phillips, R. J.; McCarthy, M. J., Measurement of the porous microstructure of hydrogels by nuclear magnetic resonance. *Journal of Colloid and Interface Science* **1995,** *174* (2), 336-344.
8. Jiang, L.; Granick, S., Real-space, in situ maps of hydrogel pores. *ACS Nano* **2016,** *11* (1), 204-212.
9. Kisley, L.; Brunetti, R.; Tauzin, L. J.; Shuang, B.; Yi, X.; Kirkeminde, A. W.; Higgins, D. A.; Weiss, S.; Landes, C. F., Characterization of porous materials by fluorescence correlation spectroscopy super-resolution optical fluctuation imaging. *ACS Nano* **2015,** *9* (9), 9158-9166.